ELSEVIER

Available online at www.sciencedirect.com

SCIENCE DIRECT®

International Journal of Solids and Structures 43 (2006) 1291–1307

INTERNATIONAL JOURNAL OF SOLIDS and STRUCTURES

www.elsevier.com/locate/ijsolstr

The dynamic behaviour of a piezoelectric actuator bonded to an anisotropic elastic medium

G.L. Huang *, C.T. Sun

School of Aeronautics and Astronautics, Purdue University West Lafayette, IN 47907, USA

Received 14 November 2004; received in revised form 4 March 2005
Available online 14 April 2005

Abstract

Surface-bonded piezoelectric actuators can be used to generate elastic waves for monitoring damages of composite materials. This paper provides an analytical and numerical study to simulate wave propagation in an anisotropic medium induced by surface-bonded piezocermic actuators under high-frequency electric loads. Based on a one-dimensional actuator model, the dynamic load transfer between a piezoceramic actuator and an anisotropic elastic medium under in-plane mechanical and electrical loading is obtained. The wave propagation induced by the surface-bonded actuator is also studied in detail by using Fourier transform technique and solving the resulting integral equations in terms of the interfacial shear stress. Typical examples are provided to show effects of the geometry, the material combination, the loading frequency and the material anisotropy of the composite upon the load transfer and the resulting wave propagation.

Keywords: Actuator; Wave propagation; Anisotropy

1. Introduction

The development of new piezoceramic materials, which are capable of generating larger strains under electric loads has revived the intense research and development of new piezoceramic actuators for different structural applications, e.g. large-scale space structures, aircraft structures, satellites, and so forth (Gandhi and Thompson, 1992; Ha et al., 1992; Varadan et al., 1993). Because of their advantages of quick response, low power consumption and high linearity, piezoelectric actuators may also be used to induce high frequency elastic wave propagation in different engineering structures for their health monitoring (Fukunaga

* Corresponding author. Tel.: +1 7654949101; fax: +1 7654940307.
E-mail address: huang39@ecn.purdue.edu (G.L. Huang).

0020-7683/$ - see front matter © 2005 Elsevier Ltd. All rights reserved.
doi:10.1016/j.ijsolstr.2005.03.010

et al., 2002 and Giurgiutiu et al., 2002). In those applications, surface-bonded actuators have the advantages that they can be attached to existing structures to form an online monitoring system and minimize the adverse effects on structures by avoiding internal weak points induced by embedded actuators for cases where the effects of these inclusions are significant. The most fundamental issue surrounding the effective use of surface-bonded piezoelectric actuators in this type of applications is the evaluation of the load transfer and the generated wave propagation for different actuator designs and arrangements, especially for the anisotropic host medium which makes evaluation of the results more difficult.

Crawley and de Luis (1987) first analyzed a beam-like structure with surface bonded and embedded thin sheet piezoelectric actuators to study the load transfer between the actuator and the host beam. In that analysis, the axial stress in the actuator was assumed to be uniform across its thickness and the host structure was treated as a Bernoulli–Euler beam. This model was further modified using a Bernoulli–Euler model of a piezoelectric actuator by considering the linear stress distribution along its thickness (Crawley and Anderson, 1990). Im and Atluri (1989) further modified the actuator model presented by Crawley and de Luis (1987) by considering both the axial and the transverse shear forces in the beam. A refined actuator model based on the plane stress condition was presented for a beam structure with symmetrically surface-bonded actuator patches (Lin and Rogers, 1993a,b). Recently, Zhang et al. (2003) presented a method to analyze a piezoelectric layer surface bonded to an isotropic elastic medium to consider the fully coupled electromechanical behaviour.

Plate and shell models have been extensively used in modeling piezoelectric structures. Wang and Rogers (1991) modified the classical laminated plate theory to model actuator-induced bending and extension of laminated plates under static loading. Tauchert (1992) further investigated the control of thermal deformation of laminated plates using piezoelectric actuators. Typical examples also include the work by Mitchell and Reddy (1995), Banks and Smith (1995), Reddy (1997), Han and Lee (1998) and Reddy (1999). Finite element method is currently also being used for active vibration and noise control of piezoelectric structures (Tzou and Ye, 1994; Lim et al., 1999; for example).

In spite of the fact that different methods have been developed to treat piezoelectric structures, existing work has mainly been focused on the global response of these systems (Wang and Meguid, 2000). Because of the difficulties association with the complicated electromechanical coupling, material inhomogeneity and anisotropy, solutions representing the dynamic local electromechanical behaviour around piezoelectric actuators have not been properly established. Recently, Wang and Huang (2001) studied the load transfer between a thin piezoelectric actuator and an anisotropic host medium for the static cases. The singular stress field around the actuator tips was studied.

The present article is concerned with the development of an analytical solution to describe dynamic coupled electromechanical behaviour of a piezoceramic actuator bonded to an infinite orthotropic elastic medium under in-plane mechanical and electrical loads, especially for high frequency cases. The actuator was characterized using a one-dimensional model. The load transfer between the piezoelectric actuator and the host structure was determined by using Fourier transform technique and solving resulting integral equations in terms of the interfacial shear stress. Specifically, two aspects of the work were examined. The first is concerned with determining the effect of the geometry, loading frequency, the material mismatch and the material anisotropy upon the load transfer between the actuator and the host structure, while the second is concerned with wave propagation in the anisotropic host medium.

2. Formulation of the problem

Consider now the plane strain problem of a thin piezoceramic actuator bonded to a homogeneous anisotropic elastic medium, as illustrated in Fig. 1. The poling direction of the actuator is along the z-axis and the half length and the thickness of the actuator are denoted a and h, respectively. A voltage between the upper

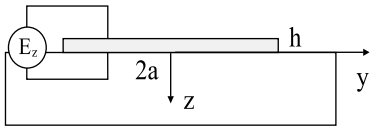

Fig. 1. An actuator surface-bonded to a host medium.

and the lower electrodes of the actuator is applied, which results in an electric field of frequency ω along the poling direction of the actuator, $E_z = (V^- - V^+)/h$. For the steady state response of the system discussed in this paper, the time factor $\exp(-i\omega t)$, which applies to all the field variables, will be suppressed.

2.1. Modelling of the actuator

Attention will be focussed on a thin-sheet actuator, for which the thickness is small compared with its length. When an electric field E_z is applied across its thickness along the poling direction, the actuator is deformed in both axial and transverse directions. Because the thickness of the actuator used is very small in comparison with its length, the applied electric field will mainly result in a deformation along the axial direction. Accordingly, the actuator can be modelled as an electroelastic element subjected to the applied electric field and the distributed interfacial stresses, as shown in Fig. 2. In this figure, τ represents the interfacial shear stress transferred between the actuator and the host medium. It is assumed that the stress σ_y^a and displacement u_y^a are uniform across the actuator. Therefore, the equation of motion of the actuator along the axial direction can be expressed as

$$\frac{d\sigma_y^a}{dy} + \tau(y)/h + \rho_a \omega^2 u_y^a = 0, \tag{1}$$

where ρ_a is the mass density of the actuator.

Under plane strain deformation, the axial stress in the actuator (σ_y^a) can be expressed as

$$\sigma_y^a = E_a \varepsilon_y^a - e_a E_z, \tag{2}$$

where E_a and e_a are effective elastic and piezoelectric material constants given in Appendix A and the strain component is given by

$$\varepsilon_y^a = \frac{du_y^a}{dy}. \tag{3}$$

Since the load transferred between the actuator and the host medium can be attributed to τ, the two ends of the actuator can be assumed to be traction free, i.e.

$$\sigma_y^a = 0, \qquad |y| = a. \tag{4}$$

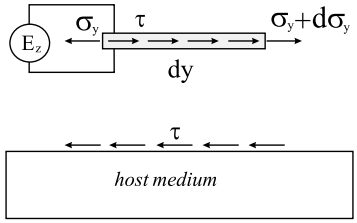

Fig. 2. Actuator model.

The axial strain and the transverse stress of the actuator can then be obtained in terms of the interfacial shear stress τ by solving Eq. (1) as

$$\varepsilon_y^{\mathrm{a}}(y) = \varepsilon_E(y) + \frac{\sin k_{\mathrm{a}}(a+y)}{hE_{\mathrm{a}} \sin 2k_{\mathrm{a}}a} \int_{-a}^{a} \cos k_{\mathrm{a}}(\xi - a)\tau(\xi)\,\mathrm{d}\xi - \int_{-a}^{y} \cos k_{\mathrm{a}}(\xi - y)\frac{\tau(\xi)}{hE_{\mathrm{a}}}\,\mathrm{d}\xi, \tag{5}$$

where

$$\varepsilon_E(y) = \frac{e_{\mathrm{a}}E_z}{E_{\mathrm{a}}} \frac{\cos k_{\mathrm{a}}y}{\cos k_{\mathrm{a}}a} \tag{6}$$

and

$$k_{\mathrm{a}} = \omega/c_{\mathrm{a}}, \quad c_{\mathrm{a}} = \sqrt{E_{\mathrm{a}}/\rho_{\mathrm{a}}} \tag{7}$$

with k_{a} and c_{a} being the wave number and the axial wave speed of the actuator, respectively.

2.2. Elastic field in the host structure

Consider now the deformation of the host orthotropic elastic medium with the principal elastic axes being parallel to y and z axes. The solution of the displacement components can be obtained by solving the governing equations of the problem using Fourier transform technique, as shown in Appendix B. The governing equations in Fourier transform domain can be expressed as

$$c_{33}\frac{\partial^2 \overline{u_y}}{\partial^2 z} + (\rho\omega^2 - c_{11}s^2)\overline{u_y} - \mathrm{i}s(c_{12}+c_{33})\frac{\partial \overline{u_z}}{\partial z} = 0, \tag{8}$$

$$c_{22}\frac{\partial^2 \overline{u_z}}{\partial^2 z} + (\rho\omega^2 - c_{33}s^2)\overline{u_z} - \mathrm{i}s(c_{12}+c_{33})\frac{\partial \overline{u_y}}{\partial z} = 0, \tag{9}$$

where c_{11}, c_{22}, c_{12} and c_{33} are material constants given in Appendix B, ω is the input loading frequency, $\overline{u_z}$ and $\overline{u_y}$ represent the displacement components along z and y directions in Fourier transform domain. The solutions of $\overline{u_z}$ and $\overline{u_y}$ are generally in the form of

$$\overline{u_z} = A\mathrm{e}^{\eta z}, \qquad \overline{u_y} = B\mathrm{e}^{\eta z}, \tag{10}$$

where A, B and η can be determined by solving the following eigenvalue problem

$$\begin{bmatrix} \omega_0^2 - c_{11}s^2 + c_{33}\eta^2 & -\mathrm{i}s\eta(c_{12}+c_{33}) \\ -\mathrm{i}s\eta(c_{12}+c_{33}) & \omega_0^2 - c_{33}s^2 + c_{22}\eta^2 \end{bmatrix} \begin{Bmatrix} A \\ B \end{Bmatrix} = 0 \tag{11}$$

with $\omega_0^2 = \rho\omega^2$.

A solution for the Eq. (11) exists only for those values of η for which the determinant of the coefficient matrix vanishes. The determinant of the above matrix, when expanded, yields the characteristic equation for η given by

$$m_1\eta^4 + m_2\eta^2 + m_3 = 0, \tag{12}$$

where

$$m_1 = c_{22}c_{33}, \tag{13}$$

$$m_2 = (2c_{12}c_{33} + c_{12}^2 - c_{11}c_{22})s^2 + (c_{22}+c_{33})\omega_0^2, \tag{14}$$

$$m_3 = (\omega_0^2 - c_{11}s^2)(\omega_0^2 - c_{33}s^2). \tag{15}$$

Eq. (12) admits four solutions for η which, because of the absence of odd-power terms, are related by

$$\eta_3 = -\eta_1, \qquad \eta_4 = -\eta_2 \tag{16}$$

with

$$\eta_1^2 = \frac{1}{2c_{22}c_{33}}[-(c_{22}+c_{33})\omega_0^2 + (c_{11}c_{22} - 2c_{12}c_{33} - c_{12}^2)s^2 + \sqrt{m}], \tag{17}$$

$$\eta_2^2 = \frac{1}{2c_{22}c_{33}}[-(c_{22}+c_{33})\omega_0^2 + (c_{11}c_{22} - 2c_{12}c_{33} - c_{12}^2)s^2 - \sqrt{m}], \tag{18}$$

$$m = d\omega_0^4 + bs^4 + 2cs^2\omega_0^2 \tag{19}$$

and

$$d = (c_{22} - c_{33})^2, \tag{20}$$

$$b = (c_{11}c_{22} - 2c_{12}c_{33} - c_{12})^2 - 4c_{11}c_{22}c_{33}^2, \tag{21}$$

$$c = 2c_{22}c_{33}^2 + 2c_{11}c_{22}c_{33} - (c_{22}+c_{33})(c_{11}c_{22} - 2c_{12}c_{33} - c_{12}^2). \tag{22}$$

The corresponding eigenvectors are obtained as

$$A = \mathrm{i}s\eta(c_{12}+c_{33})f(s), \qquad B = (\omega^2 - c_{11}s^2 + c_{33}\eta^2)f(s), \tag{23}$$

where $f(s)$ is the unknown function of s.

The principle of superposition now yields formal solutions of the form

$$\overline{u_y} = -\mathrm{i}(c_{12}+c_{33})s\eta_1 f_1(s)\mathrm{e}^{-\eta_1 z} - \mathrm{i}(c_{12}+c_{33})s\eta_2 f_2(s)\mathrm{e}^{-\eta_2 z}, \tag{24}$$

$$\overline{u_z} = (\omega^2 - c_{11}s^2 + c_{33}\eta_1^2)\mathrm{e}^{-\eta_1 z} + (\omega^2 - c_{11}s^2 - c_{33}\eta_2^2)\mathrm{e}^{-\eta_2 z}, \tag{25}$$

where the roots of (12) with positive real parts have been selected to satisfy the infinite boundary requirement for the solutions.

The transformed stresses and strains are obtained by substituting the displacements of (24) and (25) into the constitutive relations to yield

$$\overline{\sigma}_z = -[(c_{12}+c_{33})c_{12}s^2 + c_{22}(\omega^2 - c_{11}s^2 + c_{33}\eta_1^2)]\eta_1 f_1(s)\mathrm{e}^{-\eta_1 z} - [(c_{12}+c_{33})c_{12}s^2 + c_{22}(\omega^2 - c_{11}s^2 + c_{33}\eta_2^2)]\eta_2 f_2(s)\mathrm{e}^{-\eta_2 z}, \tag{26}$$

$$\overline{\sigma}_{yz} = \mathrm{i}sc_{33}[c_{11}s^2 + c_{12}\eta_1^2 - \omega^2]f_1(s)\mathrm{e}^{-\eta_1 z} + \mathrm{i}sc_{33}[c_{11}s^2 + c_{12}\eta_2^2 - \omega^2]f_2(s)\mathrm{e}^{-\eta_2 z}. \tag{27}$$

According to the present actuator model, the normal and shear stress components along the surfaces of the host medium should satisfy

$$\sigma_z(y,0) = 0, \qquad \sigma_{yz}(y,0) = -\tau. \tag{28}$$

Making use of Eqs. (26)–(28), the strain components ε_y at $z = 0$ can be expressed in terms of the shear stress τ as

$$\varepsilon_y|_{\text{matrix}} = \frac{(c_{12}+c_{33})}{2\pi c_{33}} \int_{-\infty}^{\infty} \tau(u) \int_{-\infty}^{\infty} \mathrm{i}s \frac{\eta_1 \Delta_1 + \eta_2 \Delta_2}{\Delta} \mathrm{e}^{-\mathrm{i}s(y-u)}\, \mathrm{d}s\, \mathrm{d}u, \tag{29}$$

where

$$\Delta_1(s) = s^2(c_{12}^2 + c_{12}c_{33} - c_{11}c_{22}) + c_{22}\omega^2 + c_{22}c_{33}\eta_2^2, \tag{30}$$

$$\Delta_2(s) = -[s^2(c_{12}^2 + c_{12}c_{33} - c_{11}c_{22}) + c_{22}\omega^2 + c_{22}c_{33}\eta_1^2], \tag{31}$$

$$\Delta(s) = (c_{11}s^2 + c_{12}\eta_1^2 - \omega^2)\Delta_1(s) + (c_{11}s^2 + c_{12}\eta_2^2 - \omega^2)\Delta_2(s). \tag{32}$$

2.3. Dynamic load transfer and stress distribution

The continuity between the actuator and the host structure at $z = 0$ can be described as

$$\varepsilon_y^{\mathrm{a}}(y) = \varepsilon_y(y, 0) \quad |y| < a. \tag{33}$$

By substituting Eqs. (5) and (29) into Eq. (33), the following integral equation can be obtained

$$\begin{aligned}&\frac{(c_{12}+c_{33})}{2\pi c_{33}}\int_{-\infty}^{\infty}\tau(\xi)\int_{-\infty}^{\infty}\mathrm{i}s\frac{\eta_1\Delta_1+\eta_2\Delta_2}{\Delta}\mathrm{e}^{-\mathrm{i}s(y-\xi)}\,\mathrm{d}s\,\mathrm{d}\xi - \frac{\sin k_{\mathrm{a}}(a+y)}{hE_{\mathrm{a}}\sin 2k_{\mathrm{a}}a}\int_{-a}^{a}\cos k_{\mathrm{a}}(\xi-a)\tau(\xi)\,\mathrm{d}\xi\\ &+\int_{-a}^{y}\cos k_{\mathrm{a}}(\xi-y)\frac{\tau(\xi)}{hE_{\mathrm{a}}}\,\mathrm{d}\xi\\ &=\frac{e_{\mathrm{a}}E_z}{E_{\mathrm{a}}}\frac{\cos k_{\mathrm{a}}y}{\cos k_{\mathrm{a}}a}.\end{aligned} \tag{34}$$

Asymptotic analysis of $\frac{\eta_1\Delta_1+\eta_2\Delta_2}{\Delta}$ indicates that

$$\lim_{s\to\infty}\frac{s(c_{12}+c_{33})(\eta_1\Delta_1+\eta_2\Delta_2)}{c_{33}\Delta} = \frac{1}{\overline{E}}, \tag{35}$$

where $\overline{E}$ is an effective modulus of the host medium given by

$$\overline{E} = \begin{cases} \dfrac{K_1K_2(\beta_2-\beta_1)}{(K_1+K_2)(c_{12}+c_{33})} & c_{33} < \frac{1}{2}\left(\sqrt{c_{11}c_{22}} - c_{12}\right),\\ \dfrac{\overline{K}_2^2}{\overline{\overline{K}}_1(c_{12}+c_{33})} & c_{33} = \frac{1}{2}\left(\sqrt{c_{11}c_{22}} - c_{12}\right),\\ \dfrac{\beta_4(\overline{\overline{K}}_1^2+\overline{\overline{K}}_2^2)}{\overline{\overline{K}}_1(c_{12}+c_{33})} & c_{33} > \frac{1}{2}\left(\sqrt{c_{11}c_{22}} - c_{12}\right),\end{cases} \tag{36}$$

where

$$\begin{aligned}&K_1 = -(c_{22}c_{33}\beta_2^2 - c_{11}c_{22} + c_{12}^2 + c_{12}c_{33}), \quad K_2 = (c_{22}c_{33}\beta_1^2 - c_{11}c_{22} + c_{12}^2 + c_{12}c_{33}),\\ &\overline{K}_1 = 2c_{22}c_{33}\beta_0^2, \quad \overline{K}_2 = c_{22}c_{33}\beta_0^2 - c_{11}c_{22} + c_{12}^2 + c_{12}c_{33}, \quad \overline{\overline{K}}_1 = 2\beta_3\beta_4c_{22}c_{33},\\ &\overline{\overline{K}}_2 = c_{22}c_{33}(\beta_3^2 - \beta_4^2) - c_{11}c_{22} + c_{12}^2 + c_{12}c_{13}, \quad \beta_0 = \sqrt{u_1}, \quad \beta_1 = \sqrt{u_1 + \sqrt{u_1^2 - u_2}},\\ &\beta_2 = \sqrt{u_1 - \sqrt{u_1^2 - u_2}}, \quad \beta_3 = \sqrt{\frac{\sqrt{u_2}+u_1}{2}} \quad \beta_4 = \sqrt{\frac{\sqrt{u_2}-u_1}{2}}, \quad u_1 = \frac{c_{11}c_{22} + c_{33}^2 - (c_{12}+c_{33})^2}{2c_{22}c_{33}},\\ &u_2 = \frac{c_{11}}{c_{22}}.\end{aligned}$$

Therefore, Eq. (34) is singular integral equation of the first kind, which involves a square-root singularity of τ at the ends of the actuator. The general solution of τ can be expressed in terms of Chebyshev polynomials, such that

$$\tau(y) = \sum_{j=0}^{\infty} c_j T_j(y/a)/\sqrt{1-y^2/a^2} \tag{37}$$

with T_j being Chebyshev polynomials of the first kind.

If the expansions in (37) are truncated to the (N)th term and Eq. (34) is satisfied at the following collocation points along the length of the actuator (Wang and Huang, 2001)

$$y^l = a\cos\left(\frac{l-1}{N-1}\pi\right), \quad l = 1,2,\ldots,N, \tag{38}$$

N linear algebraic equations in terms of $\{c\} = \{c_1, c_2, \ldots, c_{N-1}\}^{\mathrm{T}}$ can be obtained as

$$[Q]\{c\} = \{F\}, \tag{39}$$

where $[Q]$ is a known matrix given in Appendix C and $\{F\}$ is the applied load with

$$F_1 = \varepsilon_E(y^l) \quad l = 1,2,\ldots,N. \tag{40}$$

From these equations, the unknown coefficients in $\{c\}$ can be determined, from which the shear stress τ can be obtained.

The resulting elastodynamic field in the host medium can then be determined from the solutions of τ, using Eqs. (26) and (27), as

$$\sigma_y(y,z) = \frac{1}{2\pi}\int_{-\infty}^{\infty}\tau(\xi)\int_{-\infty}^{\infty} D_1(s)\mathrm{e}^{-\eta_1 z - \mathrm{i}s(y-\xi)}\,\mathrm{d}s\,\mathrm{d}\xi + \frac{1}{2\pi}\int_{-\infty}^{\infty}\tau(\xi)\int_{-\infty}^{\infty} D_2(s)\mathrm{e}^{-\eta_2 z - \mathrm{i}s(y-\xi)}\,\mathrm{d}s\,\mathrm{d}\xi, \tag{41}$$

$$\sigma_z(y,z) = \frac{1}{2\pi}\int_{-\infty}^{\infty}\tau(\xi)\int_{-\infty}^{\infty} D_3(s)\mathrm{e}^{-\eta_1 z - \mathrm{i}s(y-\xi)}\,\mathrm{d}s\,\mathrm{d}\xi + \frac{1}{2\pi}\int_{-\infty}^{\infty}\tau(\xi)\int_{-\infty}^{\infty} D_4(s)\mathrm{e}^{-\eta_2 z - \mathrm{i}s(y-\xi)}\,\mathrm{d}s\,\mathrm{d}\xi, \tag{42}$$

$$\sigma_{yz}(y,z) = \frac{1}{2\pi}\int_{-\infty}^{\infty}\tau(\xi)\int_{-\infty}^{\infty} D_5(s)\mathrm{e}^{-\eta_1 z - \mathrm{i}s(y-\xi)}\,\mathrm{d}s\,\mathrm{d}\xi + \frac{1}{2\pi}\int_{-\infty}^{\infty}\tau(\xi)\int_{-\infty}^{\infty} D_6(s)\mathrm{e}^{-\eta_2 z - \mathrm{i}s(y-\xi)}\,\mathrm{d}s\,\mathrm{d}\xi, \tag{43}$$

where

$$D_1(s) = \frac{-\mathrm{i}\Delta_1[s^2c_{11}(c_{12}+c_{33}) - c_{12}(c_{33}\eta_1^2 - c_{11}s^2 + \omega^2)]}{sc_{33}\Delta},$$

$$D_2(s) = \frac{-\mathrm{i}\Delta_2[s^2c_{11}(c_{12}+c_{33}) - c_{12}(c_{33}\eta_2^2 - c_{11}s^2 + \omega^2)]}{sc_{33}\Delta},$$

$$D_3(s) = \frac{-\mathrm{i}\Delta_1[s^2c_{12}(c_{12}+c_{33}) - c_{22}(c_{33}\eta_1^2 - c_{11}s^2 + \omega^2)]}{sc_{33}\Delta},$$

$$D_4(s) = \frac{-\mathrm{i}\Delta_2[s^2c_{12}(c_{12}+c_{33}) - c_{22}(c_{33}\eta_2^2 - c_{11}s^2 + \omega^2)]}{sc_{33}\Delta},$$

$$D_5(s) = \frac{\Delta_1(s^2c_{11} + c_{12}\eta_1^2 - \omega^2)}{\Delta},$$

$$D_6(s) = \frac{\Delta_2(s^2c_{11} + c_{12}\eta_2^2 - \omega^2)}{\Delta}.$$

Using the solution of τ given by Eq. (37), the integration in Eqs. (41)–(43) can be simplified as following:

$$\sigma_y(y,z) = \sum_{j=1}^{N} c_j \begin{cases} (-1)^n \int_0^{\infty} H_1(s,z)J_j(sa)\cos(sy)\,\mathrm{d}s & j = 2n+1, \\ (-1)^{n+1}\int_0^{\infty} H_1(s,z)J_j(sa)\sin(sy)\,\mathrm{d}s & j = 2n, \end{cases} \tag{44}$$

$$\sigma_z(y,z)=\sum_{j=1}^{N}c_j\begin{cases}(-1)^n\int_0^\infty H_2(s,z)J_j(sa)\cos(sy)\,\mathrm{d}s & j=2n+1,\\ (-1)^{n+1}\int_0^\infty H_2(s,z)J_j(sa)\sin(sy)\,\mathrm{d}s & j=2n,\end{cases} \tag{45}$$

$$\sigma_{yz}(y,z)=\sum_{j=1}^{N}c_j\begin{cases}(-1)^n\int_0^\infty H_3(s,z)J_j(sa)\sin(sy)\,\mathrm{d}s & j=2n+1,\\ (-1)^n\int_0^\infty H_3(s,z)J_j(sa)\cos(sy)\,\mathrm{d}s & j=2n,\end{cases} \tag{46}$$

where $H_1(s,z)$, $H_2(s,z)$, $H_3(s,z)$ are given by

$$\begin{aligned}H_1(s,z)&=D_1(s)\mathrm{e}^{-\eta_1 z}+D_2(s)\mathrm{e}^{-\eta_2 z},\\ H_2(s,z)&=D_3(s)\mathrm{e}^{-\eta_1 z}+D_4(s)\mathrm{e}^{-\eta_2 z},\\ H_3(s,z)&=D_5(s)\mathrm{e}^{-\eta_1 z}+D_6(s)\mathrm{e}^{-\eta_2 z}.\end{aligned}$$

The stress field is singular near the tips of the actuator. This singular behaviour can be characterized by a shear stress singularity factor (SSSF), S, defined by

$$\begin{aligned}S_{\mathrm{r}}&=\lim_{y\to a}[\sqrt{2\pi(a-y)}\tau(y)],\\ S_{\mathrm{l}}&=\lim_{y\to -a}[\sqrt{2\pi(a+y)}\tau(y)],\end{aligned} \tag{47}$$

with subscript 'r' and 'l' representing right and left tips, respectively.

According to this definition, the SSSF can be expressed in terms of c_j as being

$$S_{\mathrm{l}}=\sqrt{a\pi}\sum_{j=1}^{N}(-1)^j c_j,\qquad S_{\mathrm{r}}=\sqrt{a\pi}\sum_{j=1}^{N}c_j. \tag{48}$$

3. Analysis and discussion

This section will be devoted to the discussion of the load transfer from piezoelectric actuators to the host structure and the behaviour of the resulting wave propagation under different material anisotropies and loading conditions. In the following discussion, the material mismatch is defined as $q=\frac{\pi\overline{E}}{2E_{\mathrm{a}}}$ and the block stress is defined as $\sigma_{\mathrm{B}}=e_{\mathrm{a}}E_z$.

3.1. Validation of the model

To verify the validity of the current model, consider first the quasistatic behaviour of actuators bonded to an anisotropic host medium. The material constants of the actuator and the host medium are given as (Park and Sun, 1994)

Actuator

$$\begin{aligned}&c_{11}^{(\mathrm{a})}=13.9\times10^{10}\ \mathrm{Pa},\quad c_{12}^{(\mathrm{a})}=6.78\times10^{10}\ \mathrm{Pa},\quad c_{13}^{(\mathrm{a})}=7.43\times10^{10}\ \mathrm{Pa},\quad c_{33}^{(\mathrm{a})}=11.5\times10^{10}\ \mathrm{Pa},\\ &c_{44}^{(\mathrm{a})}=2.56\times10^{10}\ \mathrm{Pa},\quad e_{31}^{(\mathrm{a})}=-5.2\ \mathrm{C/m^2},\quad e_{33}^{(\mathrm{a})}=15.1\ \mathrm{C/m^2},\quad e_{15}^{(\mathrm{a})}=12.7\ \mathrm{C/m^2},\\ &\varepsilon_{11}^{(\mathrm{a})}=6.45\times10^{-9}\ \mathrm{C/Vm},\quad \varepsilon_{33}^{(\mathrm{a})}=5.62\times10^{-9}\ \mathrm{C/Vm}.\end{aligned}$$

Orthotropic medium

$$\begin{aligned}&c_{11}=13.92\times10^{10}\ \mathrm{Pa},\qquad c_{22}=160.7\times10^{10}\ \mathrm{Pa},\\ &c_{33}=7.07\times10^{10}\ \mathrm{Pa},\qquad c_{12}=6.44\times10^{10}\ \mathrm{Pa}.\end{aligned}$$

Isotropic medium

$$E = 5.4 \times 10^{11}\ \text{Pa}, \qquad v = 0.3.$$

To compare with the prediction by the current model, finite element method (FEM) is conducted using commercially available finite element code ANSYS to analyse the static stress distribution along a surface-bonded piezoelectric actuator. Two-dimensional coupled-field element (four nodes "PLANE13") with three degrees of freedom per node (u_y, u_z, V) has been chosen for both the host medium and the piezoelectric actuator. A voltage is generated across the thickness of the actuator by applying different electric potentials to nodes along the upper and lower surfaces.

It should be noted that an isotropic medium will satisfy the relation $c_{33} = \frac{1}{2}\left(\sqrt{c_{11}c_{22}} - c_{12}\right)$. For the isotropic medium, the effective modulus $\overline{E}$ in Eq. (36) will result in $\overline{E} = E/(1-v^2)$ (Wang and Meguid, 2000) and therefore the same interfacial shear stress τ^* can be obtained if the same effective modulus is used for both anisotropic and isotropic media.

In the current example, the orthotropic and isotropic media have the same effective modulus $\overline{E}$, which results in $q = 3.0$, as defined in Eq. (36). Our analytical model predicts that interfacial stress uniquely depends on q for the static cases in considering the effect of the material properties. The comparison of $\tau^* = \frac{\tau}{\sigma_B}$ in Fig. 3 for the case where the ratio between the length and the thickness of the actuator $\alpha = a/h = 20$ confirms the feasibility of the present model. It is very interesting to mention that FEM results from orthotropic and isotropic media give very close interfacial stress distributions for the same material mismatch q. The discrepancy between the analytical prediction and the FEM results may be caused by the one-dimensional assumption of the actuator.

3.2. Dynamical stress distribution along the interface

Fig. 4 shows the real part of the normalized dynamic shear stress distribution $\tau^* = \tau/\sigma_B$ along the interface between an actuator and the matrix for the same anisotropic host medium in Fig. 3 where $\alpha = a/h = 20$

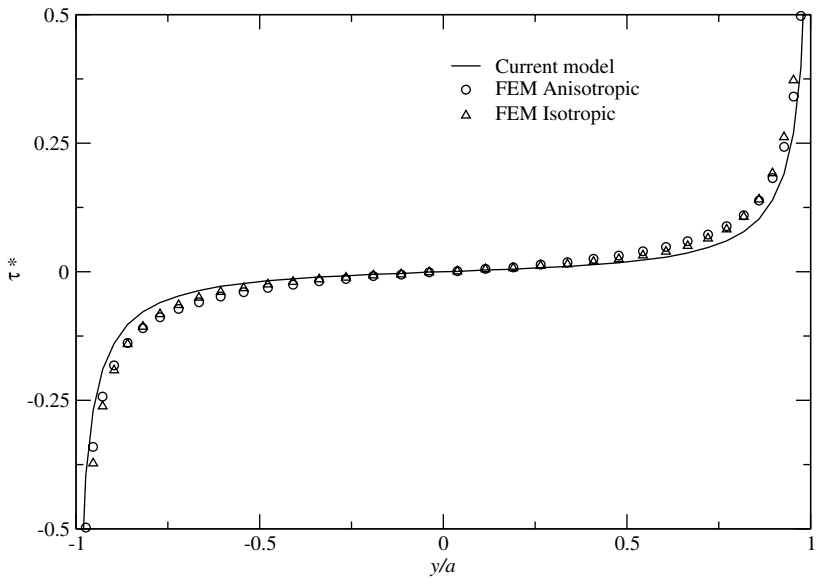

Fig. 3. Comparison of distribution of the interfacial shear stress.

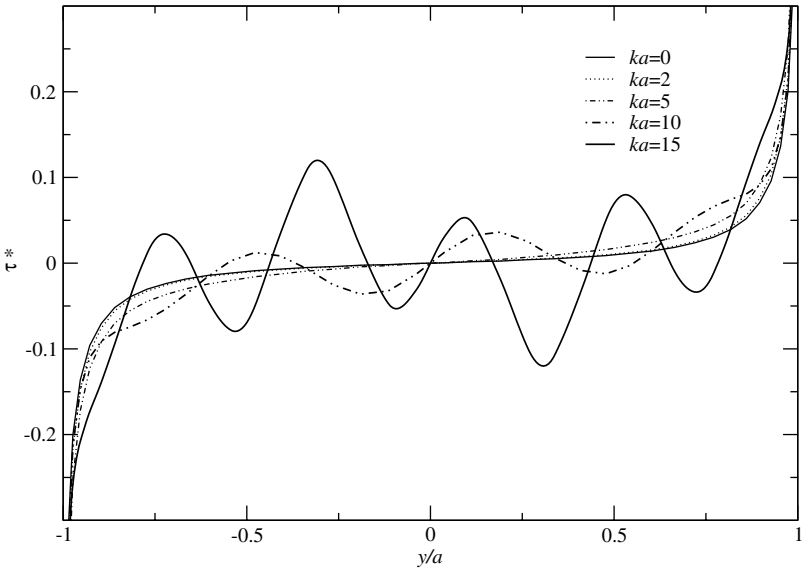

Fig. 4. Effects of loading frequency upon the interfacial shear stress.

and $\rho_a/\rho_H = 1$, with ρ_a and ρ_H being the mass density of the actuator and the host medium, respectively. The wave number (ka) shows significant effects upon the load transfer, as evidenced by the increase of the stress level in the region of $y = -0.9a$–$0.9a$ with increasing ka.

To investigate the effect of material anisotropy upon the dynamic load transfer predicted from the current model, numerical simulation is conducted. Fig. 5 shows the effect of the Poisson ratio $v_{yz} = c_{12}/c_{11}$ upon the real part of the dynamic interfacial stress τ^* for $ka = 2$, $\rho_a/\rho_H = 1$, $c_{22}/c_{11} = 3$ and $c_{33}/c_{11} = 0.1$. It can be found that the interfacial shear stress in the region of $y = 0.3a$–$0.8a$ will increase with the increase of ratio c_{12}/c_{11}. Fig. 6 shows the effect of c_{33}/c_{11} upon the real part of the dynamic interfacial stress τ^* for $ka = 2$, $\rho_a/\rho_H = 1$, $c_{22}/c_{11} = 3$ and $c_{12}/c_{11} = 0.15$. The interfacial shear stress in the region of $y = 0.3a$–$0.8a$ will decrease with the increase of the ratio c_{33}/c_{11}. Comparing the results in Figs. 5 and 6, it is interesting to note that the dynamic interfacial stress is relatively insensitive to the change of the Poisson ratio but is sensitive to the change of the shear modulus c_{33}. Fig. 7 shows the effect of c_{22}/c_{11} upon the real part of the dynamic interfacial stress τ^* for $ka = 2$, $\rho_a/\rho_H = 1$, $c_{33}/c_{11} = 0.3$ and $c_{12}/c_{11} = 0.3$. It is observed that the material anisotropy will cause a significant change on the dynamic interfacial stress, which indicates that we should consider the effects of the material anisotropy properly.

3.3. Singular stress field around the actuator

Another interesting issue is the local stress field around the tips of the actuators. The normalized dynamic stress intensity factors $S^* = S/\sigma_B\sqrt{2\pi a}$ is depicted in Fig. 8 for $ka = 2$, $\rho_a/\rho_H = 1$, $\frac{c_{12}}{c_{11}} = 0.3$ and $\frac{c_{33}}{c_{11}} = 0.3$. It shows a significant effect of the material anisotropy c_{11}/c_{22} upon the singular stress field around the tip of the actuator. With the increase of the length of the actuator (a/h), the singular field will approach a steady state, as evidenced by the fact that S^* tends to a constant for large a/h. The variation of the normalized stress intensity factors S^* is shown in Fig. 9. It is observed that the material combination q has significant effects upon the singular stress at the tips of the actuator. It is interesting to note that S^* is not sensitive to the loading frequency until ka approaches 10.

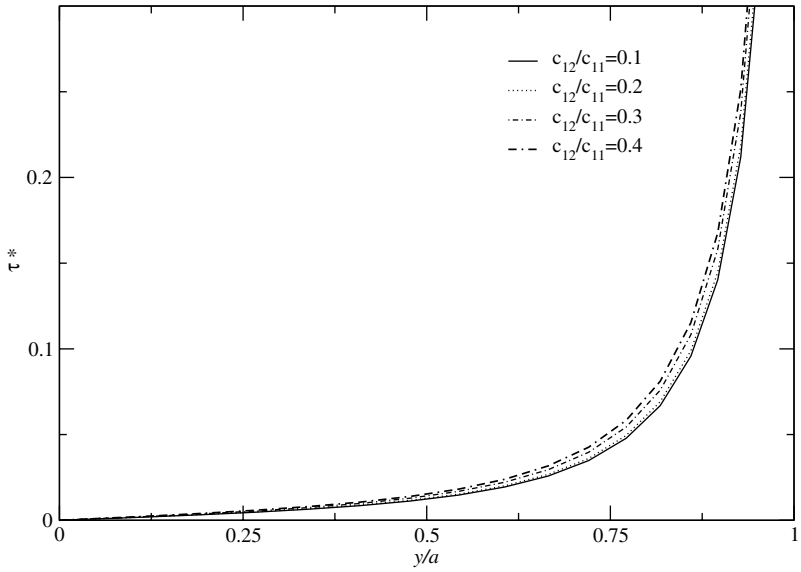

Fig. 5. Effects of Poisson ratio upon the interfacial shear stress.

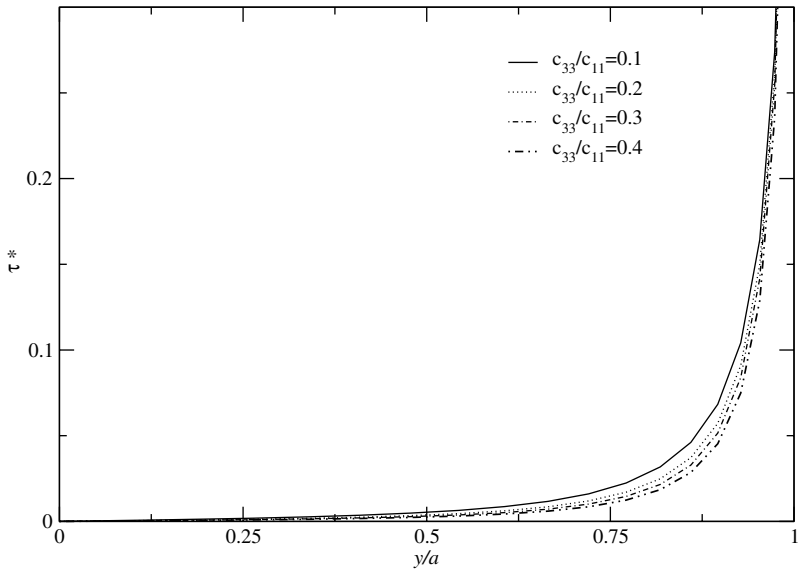

Fig. 6. Effects of c_{33}/c_{11} upon the interfacial shear stress.

3.4. Wave propagation in the host medium

Fig. 10 shows the amplitude of the resulting elastic wave propagation from a single actuator $\sigma_y^* = \sigma_y/\sigma_B$ in the host medium for $ka = 2$, $\rho_a/\rho_H = 1$, $\alpha = 10$, $\frac{c_{22}}{c_{11}} = 11.53$, $\frac{c_{12}}{c_{11}} = 0.46$ and $\frac{c_{33}}{c_{11}} = 0.51$. High stress concentration can be observed around the tips of the actuator. The stress will be reduced with the distance from the actuator and eventually generate a Rayleigh wave, which propagates with a constant amplitude along

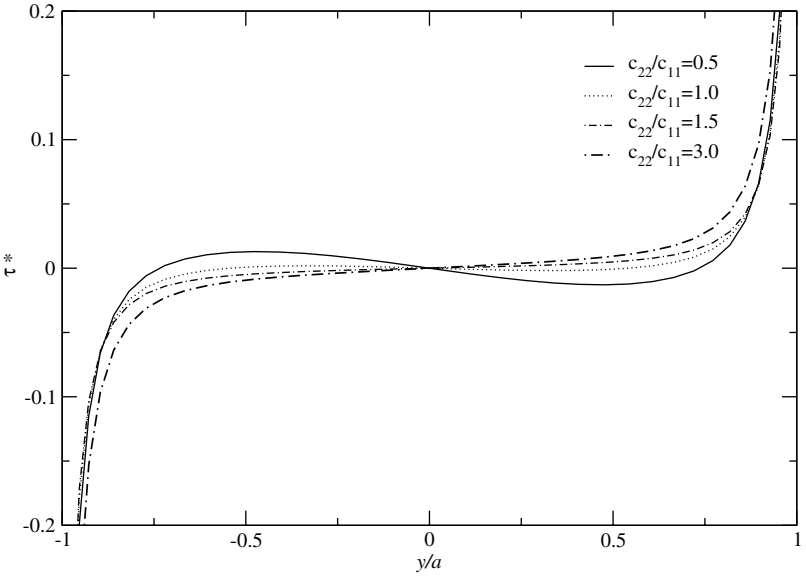

Fig. 7. Effects of c_{22}/c_{11} upon the interfacial shear stress.

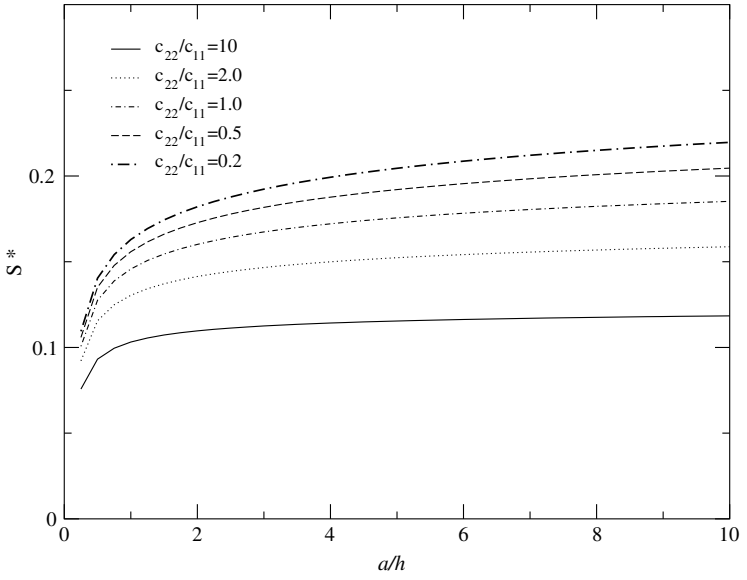

Fig. 8. The shear stress singularity factor S^*.

the surface of the matrix. Fig. 11 shows the corresponding results for $ka = 2$, $\rho_a/\rho_H = 1$, $\alpha = 10$, $\frac{c_{22}}{c_{11}} = 2.53$, $\frac{c_{12}}{c_{11}} = 0.46$ and $\frac{c_{33}}{c_{11}} = 0.51$. Comparing the wave field in Figs. 10 and 11, it can be found that the material anisotropy will have significant effects upon the resulting wave field. Fig. 12 shows the amplitude of $\sigma_y^* = \sigma_y/\sigma_B$ in the matrix caused by the same actuator and the host medium discussed in Fig. 8 for the case where $ka = 10.0$. A strong wave propagation along $\theta = 45^0$ with respect to z-direction can be

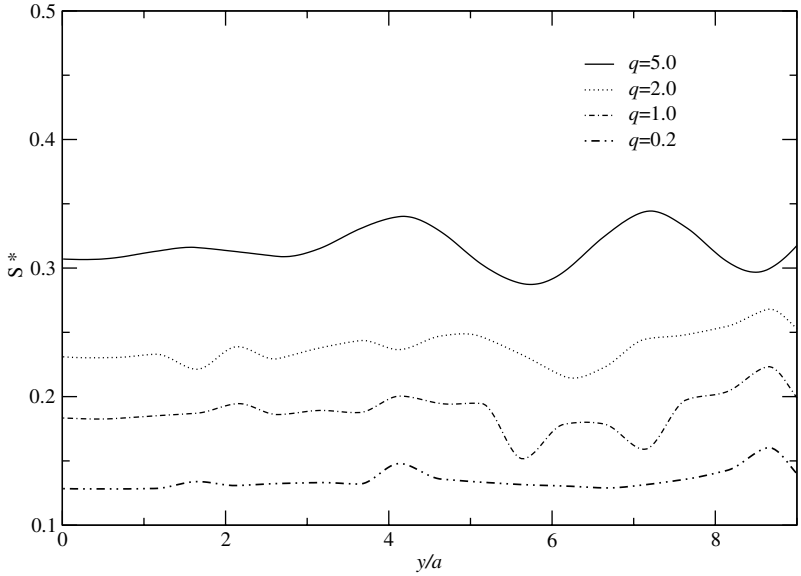

Fig. 9. The shear stress singularity factor S^*.

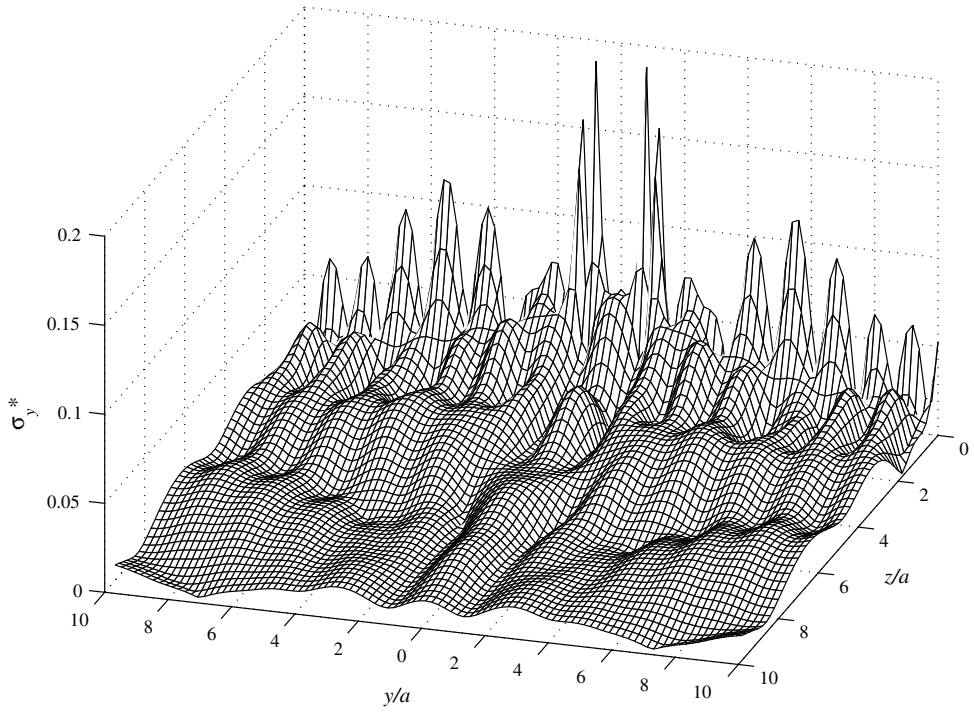

Fig. 10. Normalized local stress distribution σ_y^*.

observed. This is believed to be caused by the increase of the dynamic shear stress along the actuator-matrix interface due to high loading frequency.

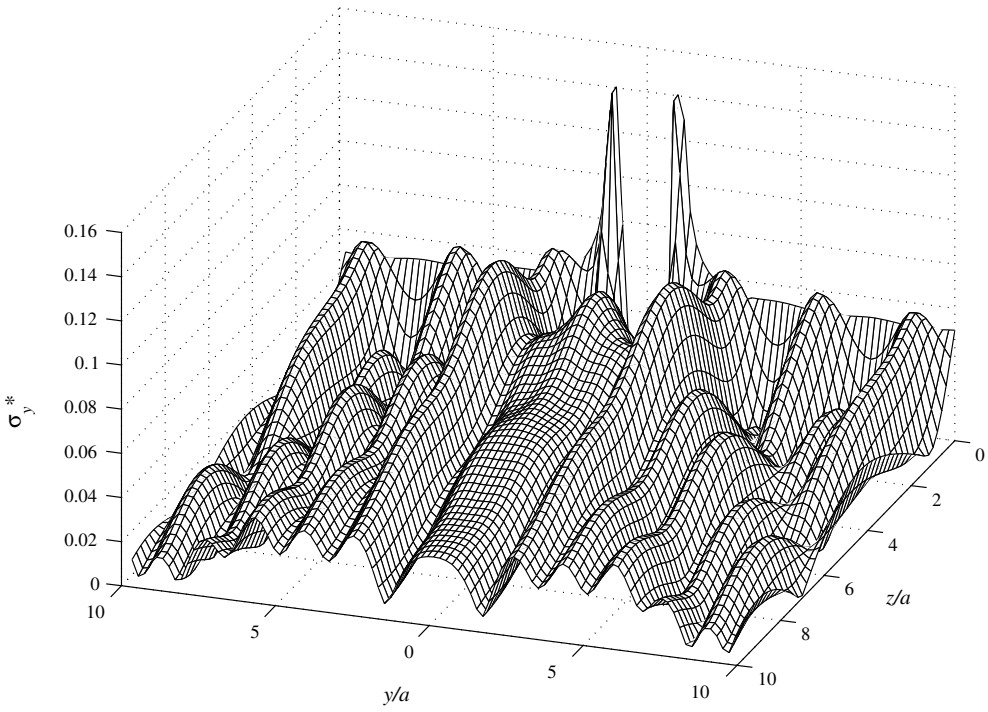

Fig. 11. Normalized local stress distribution σ_y^*.

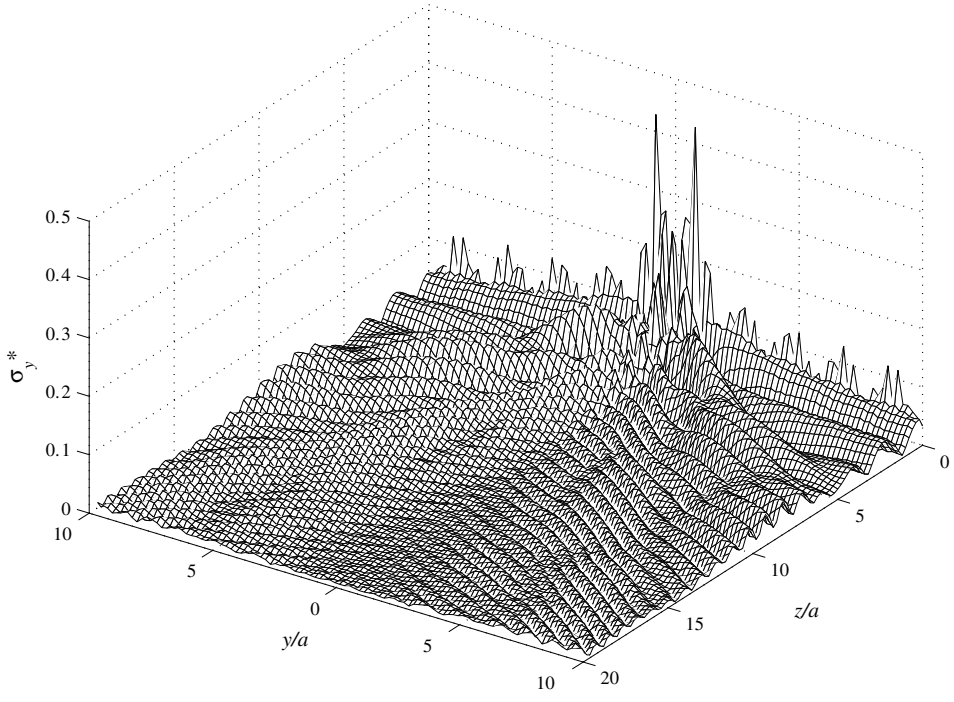

Fig. 12. Normalized local stress distribution σ_y^*.

4. Concluding remarks

A general analytical solution is provided to the dynamic coupled electromechanical behaviour of a piezoelectric actuator bonded to an orthotropic elastic medium under plane electric loading. The analysis is based upon the use of a piezoelectric line model of the actuator and the solution of the resulting singular integral equations. The validity of the present model have been demonstrated by application to specific examples and comparison with the corresponding results obtained from finite element analysis. The numerical results show effects of the geometry, the material combination, the loading frequency and the material anisotropy of the composite upon the load transfer and the resulting wave propagation.

Acknowledgment

This work was supported by the Natural Sciences and Engineering Research Council of Canada.

Appendix A. Effective material constants

The mechanical and electrical properties of piezoceramic materials can be described by

$$\{\sigma\} = [c]\{\epsilon\} - [e]\{E\}, \quad \{D\} = [e]\{\epsilon\} + [\varepsilon]\{E\},$$

where

$$\epsilon_{ij} = \frac{1}{2}(u_{i,j} + u_{j,i}), \quad E_i = -V_{,i}.$$

In these equations, $\{\sigma\}$ and $\{\epsilon\}$ are the stress and the strain fields, $\{D\}$, $\{E\}$ and V represent the electric displacement, the electric field intensity and the potential, respectively. $[c]$ is a matrix containing the elastic stiffness parameters for a constant electric potential, $[e]$ represents a tensor containing the piezoelectric constants and $[\varepsilon]$ represents the dielectric constants for zero strains.

According to the electroelastic line actuator model, $\sigma_z = 0$ and $\varepsilon_x = 0$. The effective material constants of the actuator can then be determined as

$$E_a = c_{11} - \frac{c_{13}^2}{c_{33}} \text{ plane strain},$$
$$e_a = e_{13} - e_{33}\frac{c_{13}}{c_{33}} \text{ plane strain},$$
$$\varepsilon_a = \varepsilon_{33} + \frac{e_{33}^2}{c_{33}} \text{ plane strain},$$

where the direction of polarization is designated as being the z-axis.

Appendix B. Basic solution for an orthotropic medium

If the half space shown in Fig. 1 is an orthotropic medium whose principal elastic axes (in the two dimensional case) are parallel to y and z axes, respectively, The constitutive equation is as follows:

$$\begin{Bmatrix} \sigma_y \\ \sigma_z \\ \sigma_{yz} \end{Bmatrix} = \begin{bmatrix} c_{11} & c_{12} & 0 \\ c_{12} & c_{22} & 0 \\ 0 & 0 & c_{33} \end{bmatrix} \begin{Bmatrix} \varepsilon_y \\ \varepsilon_z \\ \varepsilon_{yz} \end{Bmatrix}.$$

Using the strain–displacement relation and substituting the constitutive relation into the equilibrium equations give

$$c_{11}\frac{\partial^2 u_y}{\partial^2 y}+c_{22}\frac{\partial^2 u_y}{\partial^2 z}+(c_{12}+c_{33})\frac{\partial^2 u_z}{\partial y\partial z}=-\rho\omega^2 u_y,$$

$$c_{33}\frac{\partial^2 u_z}{\partial^2 y}+c_{22}\frac{\partial^2 u_z}{\partial^2 z}+(c_{12}+c_{33})\frac{\partial^2 u_y}{\partial y\partial z}=-\rho\omega^2 u_z.$$

Here u_z and u_y represent the displacement components along z and y directions. Applying Fourier transform with respect to y defined by

$$\overline{u_y}(s,z)=\int_{-\infty}^{\infty}u_y(y,z)\mathrm{e}^{\mathrm{i}sy}\,\mathrm{d}y,\qquad \overline{u_z}(s,z)=\int_{-\infty}^{\infty}u_z(y,z)\mathrm{e}^{\mathrm{i}sy}\,\mathrm{d}y$$

the equilibrium equations in the Fourier transform domain can be expressed as

$$c_{33}\frac{\partial^2\overline{u_y}}{\partial^2 z}+(\rho\omega^2-c_{11}s^2)\overline{u_y}-\mathrm{i}s(c_{12}+c_{33})\frac{\partial\overline{u_z}}{\partial z}=0,$$

$$c_{22}\frac{\partial^2\overline{u_z}}{\partial^2 z}+(\rho\omega^2-c_{33}s^2)\overline{u_z}-\mathrm{i}s(c_{12}+c_{33})\frac{\partial\overline{u_y}}{\partial z}=0.$$

From these equations, the two unknown functions $\overline{u_y}(s,z)$ and $\overline{u_z}(s,z)$ can be obtained, which are given in Eqs. (24) and (25).

Appendix C. Governing equations

The matrix $[Q]$ used in Eq. (39) for solving the single actuator problem is given by

$$Q_{lj}=-\frac{\pi}{\overline{E}}\sum_{j=1}^{\infty}c_j\frac{\sin[j\cos^{-1}\eta^l]}{\sin[\cos^{-1}\eta^l]}+\frac{\pi}{\overline{E}}\sum_{j=1}^{\infty}c_j\int_0^{\infty}P_j^1(\overline{s},\eta^l)\left(s\frac{\eta_1\Delta_1+\eta_2\Delta_2}{\Delta}+1\right)\mathrm{d}\overline{s}$$
$$+\frac{\alpha}{E_\mathrm{a}}v\sum_{j=1}^{\infty}c_j\int_{\cos^{-1}\eta^l}^{\pi}\cos[\overline{k_\mathrm{a}}(\cos\theta-\eta^l)]\cos(j\theta)\,\mathrm{d}\theta-\frac{\alpha}{E_\mathrm{a}}\frac{\sin[\overline{k}_\mathrm{a}(\eta^l+1)]}{\sin(2\overline{k}_\mathrm{a})}\sum_{j=1}^{\infty}c_jP_j^2.$$

In above equations,

$$\eta^l=y^l/a,\quad \overline{K}=Ka,\quad \overline{k}=ka,\quad \overline{k_\mathrm{a}}=k_\mathrm{a}a,\quad \overline{s}=sa$$

and

$$\left.\begin{aligned}P_j^1(\overline{s},\eta^l)&=J_j(\overline{s})\begin{cases}(-1)^n\cos(\overline{s}\eta^l) & j=2n+1\\ (-1)^{n+1}\sin(\overline{s}\eta^l) & j=2n\end{cases}\\ P_j^2&=J_j(\overline{k}_\mathrm{a})\begin{cases}(-1)^n\sin(\overline{k}_\mathrm{a}) & j=2n+1\\ (-1)^n\cos(\overline{k}_\mathrm{a}) & j=2n\end{cases}\end{aligned}\right\}$$

with J_j $(j=1,2\ldots)$ being the Bessel functions of the first kind.

References

Banks, H.T., Smith, R.C., 1995. The modeling of piezoceramic patch interactions with shells, plates, and beams. Quarterly of Applied Mathematics LIII, 353–381.

Crawley, E.F., Anderson, E.H., 1990. Detailed models of piezoelectric actuation of beams. Journal of Intelligent Material Systems and Structures 1, 4–25.

Crawley, E.F., de Luis, J., 1987. Use of piezoelectric actuators as elements of intelligent structures. AIAA Journal 25, 1373–1385.

Fukunaga, H., Hu, N., Chang, F.K., 2002. Structural damage identification using piezoelectric sensors. International Journal of Solids and Structures 39, 393–418.

Gandhi, M.V., Thompson, B.S., 1992. Smart Materials and Structures. Chapman & Hall, London.

Giurgiutiu, V., Zagrai, A., Bao, J., 2002. Piezoelectric wafer embedded active sensors for aging structural health monitoring. Structural Health Monitoring 1, 41–61.

Ha, S.K., Kerlers, C., Chang, F.K., 1992. Finite element analysis of composite structures containing distributed piezoelectric sensors and actuators. AIAA Journal 30, 772–780.

Han, J.-H., Lee, I., 1998. Analysis of composite plates with piezoelectric actuators for vibration control using layerwise displacement theory. Composites, Part B 29, 519–672.

Im, S., Atluri, S.N., 1989. Effects of a piezo-actuator on a finite deformation beam subjected to general loading. AIAA Journal 27, 1801–1807.

Lim, Y.-H., Gopinathan, S.V., Varadan, V.V., Varadan, V.K., 1999. Finite element simulation of smart structures using an optimal output feedback controller for vibration and noise control. Smart Materials and Structures 8, 324–337.

Lin, M.W., Rogers, C.A., 1993a. Modeling of the actuation mechanism in a beam structure with induced strain actuators. In: Proceedings of AIAA/ASCE/ASME/ASC 34th Structures, Structural Dynamics and Materials Conference, Part VI, 19–22 April, La Jolla, CA. AIAA Inc., Washington, DC, pp. 3608–3617.

Lin, M.W., Rogers, C.A., 1993b. Actuation response of a beam structure with induced strain actuators. Adaptive Structures and Material Systems AD 35, 129–139.

Mitchell, J.A., Reddy, J.N., 1995. A study of embedded piezoelectric layers in composite cylinders. ASME Journal of Applied Mechanics 62, 166–173.

Park, S.B., Sun, C.T., 1994. Crack extension in piezoelectric materials. SPIE 2189, 357–368.

Reddy, J.N., 1997. Mechanics of Laminated Composite Plates, Theory and Analysis. CRC Press, Boca Raton, FL.

Reddy, J.N., 1999. On laminated composite plates with integrated sensors and actuators. Engineering Structures 21, 568–593.

Tauchert, T.R., 1992. Piezothermoelastic behaviour of a laminated plate. Journal of Thermal Stresses 15, 25–37.

Tzou, H.S., Ye, R., 1994. Piezothermoelasticity and precision control of piezoelectric systems: theory and finite element analysis. Journal Vibration and Acoustics 116, 489–495.

Varadan, V.K., Wu, Z., Bao, X.-Q., Varadan, V.V., 1993. Light weight robot using piezoelectric motor, sensor and actuator. Adaptive Structures and Material Systems AD 35, 141–148.

Wang, X.D., Huang, G.L., 2001. The electromechanical behaviour of a piezoelectric actuator bonded to an anisotropic elastic medium. International Journal of Solids and Structures 38, 4721–4740.

Wang, X.D., Meguid, S.A., 2000. On the electroelastic behaviour of a thin piezoelectric actuator attached to an infinite host structure. International Journal Solids and Structures 37, 3231–3251.

Wang, B.-T., Rogers, C.A., 1991. Laminate plate theory for spatially distributed induced strain actuators. Journal of Composite Materials 25, 433–452.

Zhang, J., Zhang, B., Fan, J., 2003. A coupled electromechanical analysis of a piezoelectric layer bonded to an elastic substrate: Part I, Development of governing equations. International Journal of Solids and Structures 40, 6781–6797.